Original scientific paper

Informacije MIDEM
Journal of Microelectronics,
Electronic Components and Materials
Vol. 46, No. 4(2016), 267 – 275

Combined optical model for micro-structured organic light-emitting diodes

Milan Kovačič[1], Paul-Anton Will[2], Benjamin Lipovšek[1], Janez Krč[1], Simone Lenk[2], Sebastian Reineke[2], and Marko Topič[1]

[1]University of Ljubljana, Faculty of Electrical Engineering, Ljubljana, Slovenia
[2]Technische Universität Dresden, Dresden Integrated Center for Applied Physics and Photonic Materials (IAPP) and Institute for Applied Physics, Dresden, Germany

Abstract: Organic light-emitting diodes (OLEDs) with prospect of low cost, high efficiency and high quality lighting are a promising future light source. One of their limitations is poor light outcoupling, reaching only 20-30 % for conventional flat-plate lighting devices. Optical modelling and simulations are of great importance in optimizing the outcoupling efficiency. Complex structures of OLEDs, in which thin layers with emitting sources are combined with thick texturized substrate layers, require coupled optical modelling approach. We developed a combined optical model, comprising a thin layer stack where light is described as waves and thick texturized layers where light is described as rays. This combination enables simulation of OLEDs as complete devices with micro textures. We present the main considerations of the developed model. Finally, an OLED with laser structured sine textures is used to compare experimental results with simulation results obtained with the developed model.

Keywords: OLED; organic light emitting diode; optical modeling; light outcoupling

Združeni optični model za mikrostrukturirane organske svetleče diode

Izvleček: Organske svetleče diode (OLED) predstavljajo obetajoč svetlobni vir, ki ga lahko uporabimo tudi pri razsvetljavi prostorov. Predvidena nizkocenovna proizvodnja visoko učinkovitih OLED omogoča izdelavo svetil z velikimi površinami. Ena izmed glavnih omejitev sodobnih OLED je nizka stopnja učinkovitosti izstopa svetlobe iz tankoplastne strukture elementa. Konvencionalne izvedbe OLED z gladkimi površinami dosegajo le 20-30 % stopnjo učinkovitosti izstopa svetlobe. Pomembno vlogo pri načrtovanju in optični optimizaciji struktur OLED igra optično modeliranje v povezavi z numeričnimi simulacijami. Strukture OLED združujejo tanke organske plasti v kombinaciji z debelejšimi plastmi (substrati), zato pri simulaciji potrebujemo poseben, združen optični model, ki omogoča koherentno in nekoherentno širjenje svetlobe. Razvili smo tridimenzionalni združeni optični model, kjer tanke plasti z optičnimi viri lahko obravnavamo skupaj z debelejšimi plastmi, ki hkrati vsebujejo teksture za izboljšanje učinkovitosti izstopa svetlobe. Ta kombinacija nam tako omogoča simulacije in optično optimizacijo celotnih OLED struktur, ki vsebujejo mikroteksturirane površine. V prispevku so predstavljene glavne lastnosti modela. Rezultate simulacij z razvitim modelom validiramo z izdelanimi vzorci, kjer smo teksture izdelali z laserskim graviranjem steklenega substrata.

Ključne besede: OLED; organske svetleče diode; optično modeliranje; ekstrakcija svetlobe

** Corresponding Author's e-mail: milan.kovacic@fe.uni-lj.si*

1 Introduction

Over 20 % of the generated electrical power in the developed countries and a considerable amount in the developing countries is used for lighting and the consumption will continue to grow [1]. Therefore, efficient lighting is one of the cornerstones of reducing the carbon footprint for achieving a greener future. One of the emerging lighting technologies called organic light-emitting diodes (OLEDs), offers high possibilities of becoming a future lighting source, since it is a thin film, large area (and not point source like their inorganic equivalents) lightweight device with a potential to provide low cost, highly efficient and high quality general lighting [2–4]. Similar to the limited conversion efficiency of photovoltaic devices or laser power converters [5, 6], OLEDs are also facing theoretical limits. One of the main obstacles for OLEDs to reach their full potential is poor light outcoupling, as for normal

devices only ~20-30 % of the generated light reaches the far field as useful light [7, 8], while the internal conversion efficiency from an injected electron to a generated photon is close to 100 % [9–11]. Intensive research has been done in the last years to reduce the optical losses in OLEDs, see for example [12–14], but a lot of room for improvement still remains. OLEDs are optically relatively complex devices, where even planar devices include combination of thin and thick layers, a microcavity effect, a different orientation of emitting dipoles – anisotropy, coupling of light to surface plasmon polaritons (SPP), an arbitrary angular distribution of emitted light, absorption in layers and others. Therefore, optical modelling and simulations are an essential tool in design and optimization of these devices. In this article, we present an optical model that we developed for a three-dimensional (3D) simulation of OLED structures including micro textures for efficient control of light. The model couples emitting sources (dipoles) in thin organic layers with thin-film optics of surrounding layers, ray tracing in thick incoherent layers and at micro textured surfaces. The physics of the model will be presented, followed by selected examples of validation on realistic OLED structures.

2 Optical model

2.1 OLED structure and operation

A conventional bottom-emitting p-i-n OLED structure is presented in Figure 1. It consists of a thin layer stack,

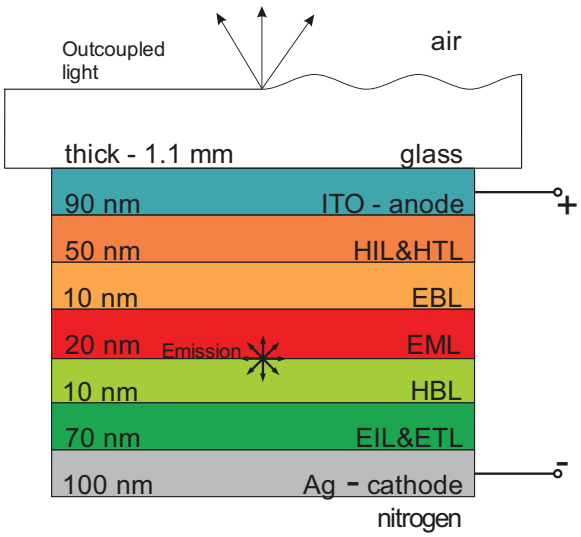

Figure 1: Structure of a conventional p-i-n bottom-emitting red OLED deposited on a glass substrate and encapsulated under a nitrogen atmosphere. Texturization of the substrate (on light escaping side) is indicated on the right hand side of the substrate.

containing light emission sources and a thick transparent substrate, e.g. glass or transparent foil that can be non-structured or structured.

Light is generated in thin emission layer (EML) by radiative recombination of electrons and holes. To ensure good supply of both, optional electron- and hole-transport (ETL, HTL), injection (EIL, HIL) and blocking layers (EBL, HBL) are added and contacted with an opaque highly reflective silver cathode and a transparent indium tin oxide (ITO) anode as shown in Figure 1.

The thicknesses of thin layers are in the range of light wavelengths therefore the light has to be treated coherently, in terms of electromagnetic waves. In thicker layers (e.g. the transparent substrate) the light has to be treated incoherently, in terms of rays.

The overall OLED device efficiency, including optical and electrical performance, can be presented by the external quantum efficiency (*EQE*) [15, 16], which is the ratio between the number of photons reaching the far field as useful light to the number of injected charge carriers:

$$EQE = \gamma \int_{\lambda} s_{\mathrm{el}}(\lambda)\, \eta^{*}_{\mathrm{rad,e}}(\lambda)\, \eta_{\mathrm{out}}(\lambda)\, d\lambda \tag{1}$$

$$\eta^{*}_{\mathrm{rad,e}}(\lambda) = \frac{\eta_{\mathrm{rad,e}} F(\lambda)}{1 - \eta_{\mathrm{rad,e}} + \eta_{\mathrm{rad,e}} F(\lambda)} \tag{2}$$

$$\eta_{\mathrm{out}} = \frac{U(\lambda)}{F(\lambda)} \tag{3}$$

Where s_{el} is a normalized luminescence spectrum of the emitting material ($\int_{\lambda} s_{\mathrm{el}}(\lambda)\, d\lambda = 1$), γ is the electrical efficiency and $\eta^{*}_{\mathrm{rad,e}}$ is the effective radiative efficiency of the emitter. Its definition is given in Eq. (2), in which $\eta_{\mathrm{rad,e}}$ is the intrinsic radiative efficiency of the emitter and $F(\lambda)$ is the total radiated power at the emitter location relative to the power radiated in an infinite homogeneous medium (also called the Purcell factor). Finally η_{out} in Eq. (1) is the outcoupling efficiency that is defined in Eq. (3) as the ratio of the total radiated power outcoupled from the OLED structure to the far field (usually air), $U(\lambda)$, to the total Purcell factor, $F(\lambda)$. Looking back to Eqs. (1)-(3), we can see that the optical properties of *EQE* are fully defined by $U(\lambda)$ and $F(\lambda)$ parameters. An optical model should therefore determine these two parameters ($U(\lambda)$ and $F(\lambda)$), while also provide an insight in optical behavior inside and outside the structure.

2.2 Concept of the model

Our model combines two sub-models: a thin-film optical model with light sources and a ray-tracing model - Figure 2. The thin-film model is based on a transfer matrix model (TMM), in which we incorporate internal light sources, in form of dipoles (as commonly used to describe light generation in organic layers) or in any other arbitrary form of light sources. The ray-tracing model is a 3D model utilized in CROWM simulator [17]. The ray-tracing model of the simulator was upgraded with TMM to be able to include thin-layer stacks also outside the OLED device (e.g. on the front side of the device, in general). The TMM approach requires that the thin layers are locally flat and plane parallel. Applied textures with micrometer dimensions (dimensions larger than light wavelengths of interest) still fulfill this condition, thus our model enables us to include micro textures either on the surface or at internal interfaces of OLED structures (see Figure 2). In the following sections, we present the main properties of the developed simulation model with governing equations and main specifics.

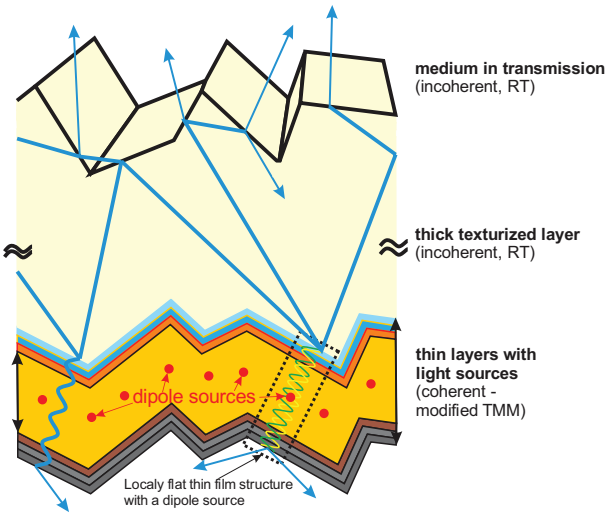

Figure 2: Combined OLED model, combining thin film layers containing dipole sources (locally flat TMM model) with thick incoherent layers (CROWM).

2.3 TMM with internal light sources

Organic layers and the thin film contacts in the OLED structure are stacks of locally flat plane parallel coherent layers. To describe the light behavior in these stacks without particular light sources at the first stage, TMM presents an efficient solution for the calculation of the optical properties inside and outside the stack. Most commonly, TMM is used for modelling of thin-film optical devices with an external light source (e.g. an illuminated flat solar cell), while in the OLEDs, the light is generated inside the thin-film structure. Therefore, to incorporate such an internal light source, we modified the TMM formulation to properly describe the light generation and propagation in a thin layer stack. A similar approach has been presented in [18].

Following the TMM formalism from [19], a plane wave propagating obliquely through the thin-film stack under some angle ϑ_i can first be separated according to its polarization – we differentiate between the transverse-electric (TE) and the transverse-magnetic (TM) polarizations, based on the plane of incidence and the orientation of the electric and magnetic fields. Next, for each of the two polarizations, the waves are further distributed into two components: the transverse plane wave component that is travelling perpendicularly to the flat interfaces through the stack, and the component that is travelling in parallel along the interfaces. TMM formalism treats only the transverse components which interact (interfere) constructively or destructively with each other, while information about the full wave is contained in the propagating angle. The electric field that belongs to the transverse wave component of emission source (incident light or internal source) is calculated separately for the TE and TM polarization for emission as:

$$E_{\mathrm{emi}}^{\mathrm{T,TE}} = E^{\mathrm{TE}} \quad E_{\mathrm{emi}}^{\mathrm{T,TM}} = E^{\mathrm{TM}} \cos\vartheta_{\mathrm{emi}} \tag{4}$$

where ϑ_{emi} is the incident angle of the total electric field incident on interfaces. In the following formulation, all the electric fields in the equations are considered to be the electric fields that belong to the transverse wave component, as denoted by the superscript T, and can originate from either the TE or the TM polarization, thus all further presented formulations need to be considered separately for TE and TM polarizations as specified in TMM formulations [19].

A thin-film layer structure, that is described by the layer thicknesses and by the corresponding complex refractive indices of the individual layers, can be defined by a TMM formalism using the product of propagation matrices *P* (propagation through layer) and matching matrices *M* (reflection and transmission at the interface) [19]. The matching matrices (*M*) are obtained by Fresnel's transverse reflection (r_j^{T}) and transverse transmission (t_j^{T}) coefficients (separately for TE and TM) at *j*-th interface as:

$$\begin{bmatrix} E_{\mathrm{j,l}}^{\mathrm{T}+} \\ E_{\mathrm{j,l}}^{\mathrm{T}-} \end{bmatrix} = \frac{1}{t_{\mathrm{j}}^{\mathrm{T}}} \begin{bmatrix} 1 & r_{\mathrm{j}}^{\mathrm{T}} \\ r_{\mathrm{j}}^{\mathrm{T}} & 1 \end{bmatrix} \cdot \begin{bmatrix} E_{\mathrm{j,r}}^{\mathrm{T}+} \\ E_{\mathrm{j,r}}^{\mathrm{T}-} \end{bmatrix} = \left[M_{\mathrm{j}} \right] \cdot \begin{bmatrix} E_{\mathrm{j,r}}^{\mathrm{T}+} \\ E_{\mathrm{j,r}}^{\mathrm{T}-} \end{bmatrix} \tag{5}$$

where $E_{\mathrm{j,l}}^{\mathrm{T}\pm}$ and $E_{\mathrm{j,r}}^{\mathrm{T}\pm}$ are electric fields on the left and right side of the *j*-th interface, respectively, propagating in the positive (+) or the negative (–) direction.

Propagation matrices (*P*) are obtained by propagating the above fields through the *k*-th layer as:

$$\begin{bmatrix} E_{\mathrm{k,l}}^{\mathrm{T}+} \\ E_{\mathrm{k,l}}^{\mathrm{T}-} \end{bmatrix} = \begin{bmatrix} e^{j\delta_{\mathrm{k}}} & 0 \\ 0 & e^{-j\delta_{\mathrm{k}}} \end{bmatrix} \cdot \begin{bmatrix} E_{\mathrm{k,r}}^{\mathrm{T}+} \\ E_{\mathrm{k,r}}^{\mathrm{T}-} \end{bmatrix} = \left[P_{\mathrm{k}}\right] \cdot \begin{bmatrix} E_{\mathrm{k,r}}^{\mathrm{T}+} \\ E_{\mathrm{k,r}}^{\mathrm{T}-} \end{bmatrix} \tag{6}$$

Where δ_{k} contains the information about the phase change and the absorption inside the layer, via the layer thickness and the complex refractive index of the layer material. A more detailed explanation and derivation of *P* and *M* matrices can be found in [19].

In the case of devices with internal sources (e.g. OLEDs), the initial electric field (presenting the emission source) is generated inside the thin film structure, namely inside a specified layer. We assume the sources are located on a plane parallel to the interfaces. More detailed emission source definition for OLED sources (dipoles) is presented in the next subchapter. To incorporate the initial electric field of the source, we put a new virtual interface parallel to the existing interfaces inside the specified layer (*m*) at an arbitrary position. The position of this virtual interface is defined by the spatial position parameter *p* as shown in eq. (7). The interface splits the original (*m*-th) layer into two layers with their thicknesses defined by *p* parameter (0 < *p* < 1) as:

$$d_{\mathrm{v,l}} = d_{\mathrm{m}} * p \; d_{\mathrm{v,r}} = d_{\mathrm{m}} * \left(1 - p\right) \tag{7}$$

Where $d_{\mathrm{v,l}}$ and $d_{\mathrm{v,r}}$ are the thicknesses of the left and the right part of the *m*-th layer after the splitting, respectively.

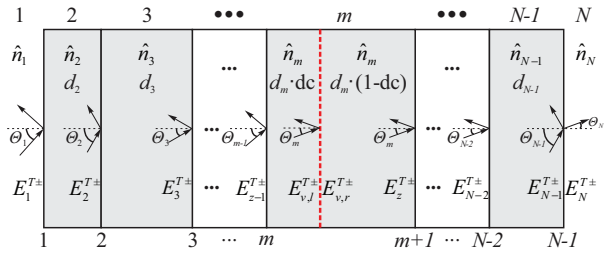

Figure 3: Schematic representation of a thin-film multilayer stack with an additional virtual interface incorporating an internal source in arbitrary layer *m*.

New electric fields (equation (4)) are introduced at the new virtual interface "*v*", their values are defined by particular emitting sources. This initial source waves are propagating away of the interface, therefore we have on the left side of the interface a source wave in negative direction ($E_{\mathrm{emi}}^{\mathrm{T}-}$) and on the right side in positive direction ($E_{\mathrm{emi}}^{\mathrm{T}+}$). Considering that the virtual interface is placed within the layer we can write the following relations:

$$E_{\mathrm{v,r}}^{\mathrm{T}+} = E_{\mathrm{v,l}}^{\mathrm{T}+} + E_{\mathrm{emi}}^{\mathrm{T}+} \; E_{\mathrm{v,l}}^{\mathrm{T}-} = E_{\mathrm{v,r}}^{\mathrm{T}-} + E_{\mathrm{emi}}^{\mathrm{T}-} \tag{8}$$

To describe these new conditions at the virtual interface, we split the entire optical system into two parts, the first part describing the thin film environment on the left of the virtual interface, and second on the right. The thin film stack on the left of the virtual interface can thus be described as:

$$\begin{bmatrix} E_1^{\mathrm{T}+} \\ E_1^{\mathrm{T}-} \end{bmatrix} = \begin{bmatrix} 0 \\ E_1^{\mathrm{T}-} \end{bmatrix} = \left[M_1\right] \cdot \left[P_2\right] \left[M_2\right] \cdot \ldots \cdot \left[M_{\mathrm{m-1}}\right] \cdot \left[P_{\mathrm{m}}^{*}\right] \cdot \begin{bmatrix} E_{\mathrm{v,l}}^{\mathrm{T}+} \\ E_{\mathrm{v,l}}^{\mathrm{T}-} \end{bmatrix} = \begin{bmatrix} B_{11} & B_{12} \\ B_{21} & B_{22} \end{bmatrix} \cdot \begin{bmatrix} E_{\mathrm{v,r}}^{\mathrm{T}+} \\ E_{\mathrm{v,r}}^{\mathrm{T}-} \end{bmatrix} \tag{9}$$

and on the right of the virtual interface as:

$$\begin{bmatrix} E_{\mathrm{v,r}}^{\mathrm{T}+} \\ E_{\mathrm{v,r}}^{\mathrm{T}-} \end{bmatrix} = \left[P_{\mathrm{m}}^{**}\right] \cdot \left[M_{\mathrm{m}}\right] \left[P_{\mathrm{m+1}}\right] \cdot \ldots \cdot \left[P_{\mathrm{N-1}}\right] \cdot \left[M_{\mathrm{N-1}}\right] \begin{bmatrix} E_{\mathrm{N}}^{\mathrm{T}+} \\ E_{\mathrm{N}}^{\mathrm{T}-} \end{bmatrix} = \begin{bmatrix} F_{11} & F_{12} \\ F_{21} & F_{22} \end{bmatrix} \cdot \begin{bmatrix} E_{\mathrm{N}}^{\mathrm{T}+} \\ 0 \end{bmatrix} \tag{10}$$

where P_{m}^{*} and P_{m}^{**} – are modified propagation matrices due to the change of thicknesses due to introducing a new virtual interface. Additionally, as the source is inside the thin film structure and no incident light from the outside is considered, the transversal electric fields representing the incoming light from the outside of the thin film structure ($E_1^{\mathrm{T}+}$ and $E_{\mathrm{N}}^{\mathrm{T}-}$) are set to 0.

Using equations (8), (9) and (10), it is straightforward to calculate the new conditions ($E_{\mathrm{v,l(r)}}^{\mathrm{T}\pm}$) at the virtual interface due to the introduced emission source ($E_{\mathrm{emi}}^{\mathrm{T}\pm}$) in the entire thin film system. Here we present the final results for superimposed fields at the position of the virtual interface only (either for TE or TM polarisation):

$$\begin{aligned} E_{\mathrm{v,r}}^{\mathrm{T}+} &= \frac{F_{11}}{B_{11} \cdot F_{11} + B_{12} \cdot F_{21}} * \left(B_{11} \cdot E_{\mathrm{emi}}^{\mathrm{T}+} - B_{12} \cdot E_{\mathrm{emi}}^{\mathrm{T}-}\right) \\ E_{\mathrm{v,r}}^{\mathrm{T}-} &= \frac{-B_{12} \cdot F_{21}}{B_{11} \cdot F_{11} + B_{12} \cdot F_{21}} * \left(E_{\mathrm{emi}}^{\mathrm{T}-} + E_{\mathrm{emi}}^{\mathrm{T}+}\right) \end{aligned} \tag{11}$$

It is worth noting that due to dipole emission symmetry $E_{\mathrm{emi}}^{\mathrm{T}+} = E_{\mathrm{emi}}^{\mathrm{T}-}$, the presented formulations are nevertheless applicable also to non-symmetric sources.

Once we determine the fields at the virtual interface, that represent source fields $E_{\mathrm{v,l(r)}}^{\mathrm{T}\pm}$, the electric fields at all other interfaces can be easily calculated using the standard TMM formulations [19]. In the final step we calculate the total E^{T} and H^{T} fields at each interface as:

$$\begin{bmatrix} E_{\mathrm{i}}^{\mathrm{T}} \\ H_{\mathrm{i}}^{\mathrm{T}} \end{bmatrix} = \begin{bmatrix} E_{\mathrm{i,t}}^{\mathrm{T}+} + E_{\mathrm{i,t}}^{\mathrm{T}-} \\ \frac{1}{\eta_{\mathrm{i}}} \left(E_{\mathrm{i,t}}^{\mathrm{T}+} - E_{\mathrm{i,t}}^{\mathrm{T}-}\right) \end{bmatrix} \tag{12}$$

where η_{i} is the material impedance connecting E^{T} and H^{T} field in the specific material. As $E_{\mathrm{v,l(r)}}^{\mathrm{T}\pm}$ are modified by

forward and backward matrices (optical environment), all the results will be relative, to the modified source expressed with the conditions at the virtual layer (not to the original input emission source). Using E^T and H^T fields, we simply calculate the total power densities of the wave entering the *i*-th layer by using the Poynting vector as:

$$P_i = \frac{1}{2} Re\left(E_i^T \times H_i^{T*}\right) / \cos\left(\vartheta_i\right) \quad (13)$$

Here, $\cos(\vartheta_i)$ is added to the classic Poynting vector formulation to obtain the power of the complete wave propagating under an oblique angle ϑ_i through the *i*-th layer. Finally, due to the modified source, expressed with the conditions at the virtual interface, all power densities must be normalized with respect to the total power density that exist on both sides of the virtual interface and corresponds to the total emission power of the source ($P_{emi,tot}$). By knowing the relative power entering each layer we can simply calculate the relative absorption (A_i) in each layer. And finally, the relative power of the light that exits the thin film stack at the left and the right side of the stack correspond to P_1 and P_N, respectively.

2.4 Definition of internal light sources

In the case of OLEDs, the electroluminescent emission is considered as a dipole transition from an excited molecular state to the ground state [20]. The sizes of the emitting sources in OLEDs do not exceed a few nanometers, being very small with respect to the wavelength, thus they can be approximated by point dipoles [20]. Point dipole emitters are in the model simulated as a classical, continuously oscillating dipole sources with predefined spectrum and angular intensity distribution (AID). The AID of a dipole in infinite medium is presented in Figure 4. The 3D AID and the two cross-sections with the corresponding angular functions are presented for the vertically oriented dipole (see black arrow). From here on the dipole orientation (vertical, horizontal) is referred to with respect to the interface planes of the structure. If the dipole is rotated, its AID rotates accordingly. Once it is put inside a thin-film multilayer structure, interference effects with reflected waves have to be considered (included in TMM).

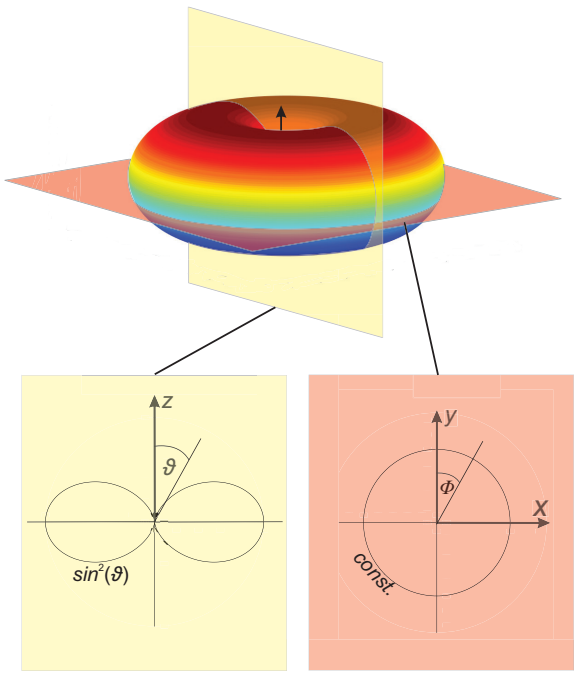

Figure 4: Vertically (according to the *xy* plane) oriented dipole in homogeneous space, with cross-sectional projections showing polar (θ) and azimuth (Φ) angles.

As dipoles emit light as spherical waves, which is not very useful in TMM formulations, their emission is converted through Fourier decomposition into plane waves travelling under specified angles. These angles may be real or imaginary valued, according to Fourier decomposition [20]. The imaginary components represent evanescent waves, which are also taken into account in the TMM.

Emitting sources (dipoles) are considered to be isotropically orientated in the plane of the layered system, thus only orientation with respect to the layered system normal has to be considered. Any arbitrary oriented dipole is decomposed into three orthogonal dipoles in the model, two parallel (horizontal) and one perpendicular (vertical) dipole, defined by their orientation to the interfaces of the planar system and the corresponding emission polarization. Special care has to be taken when defining the TE and TM components of the planar waves approaching the interfaces at different incident angles. While the magnetic field is always perpendicular to the dipole orientation, the electric field lies in the plane which is defined by dipole orientation and the direction of wave propagation. Another condition is that magnetic field, electric field and the propagation direction are perpendicular to each other. Based on these rules TE and TM components can be defined in the model.

In the OLED, the emitting layer is combined from multiple randomly oriented dipoles that can in general have some preferential orientation to the layered system normal, this can be a consequence of material properties or deposition methods (e.g. sputtering, spin coating). This preferential orientation of dipoles can be incorporated in anisotropy coefficient *a*, as a ratio between the number of vertical dipoles to the number of all dipoles. In the case of random orientation of dipoles,

a = 1/3, meaning that contributions from all three orthogonal dipoles (two horizontal and one vertical as defined above) are considered equally. Incorporating anisotropy reduces the highly complex problem of describing detailed dipole orientation to a rather simple problem of defining the fraction of parallel and perpendicular dipole moments [20].

For complete optical description of emission source (dipole), TTM approach described in previous subchapter needs to be applied for all discretized Fourier plane waves defining the (dipole) source. The ratio of total emitted power in layered system and total emitted power of the same source in an infinitive medium is the Purcell factor for a given wavelength, $F(\lambda)$, and is our first important optical parameter that can be defined by simulation.

2.5 Combining TMM model with the ray tracing simulator CROWM

A simple flat structure with a single thick layer can be easily simulated using an expanded TMM formulation that also considers incoherent light propagation through the thick flat layer [21]. However, a problem occurs when we introduce more complicated structures, e.g. such as structures with textured surfaces of the thick layer or with additional thin layers on top of the substrate. To overcome this problem, we combined our TMM model with the optical simulator CROWM [17] that enables complete optical simulation of advanced structures including thin and thick layers with or without textures. This way, it is possible to simulate arbitrary complex LED devices with flat or micro-textured substrates as well as with additional thin-film stacks incorporated in the device, such as antireflection layers etc. The simulation initiates by calculating the output of the developed TMM model with internal sources (relative powers P_1 and P_N, their angles of propagation and TE/TM decomposition), which are then taken as the input into the general CROWM simulation (combination of ray tracing and classical TMM). While the polar angles (ϑ) are defined with TMM formulations, the azimuth angles (Φ) are, due to assumed z-axis symmetry and under the assumption of isotropically oriented dipoles in a planar layer, equally distributed over possible discrete values (0-360°). Each discrete part is then considered as a ray (separately for TE and TM) and traced through the rest of the structure until it is either extracted to air or reabsorbed in the structure. Additionally, since sources are considered as point sources in a locally flat structure, a large number of sources distributed across the entire area of the device (see Figure 2) are considered, and the final result is an average of all the contributions, ensuring realistic representation of the real device.

2.6 Model limitation and advantages

The thin-film model with emission sources is considered locally flat and anisotropic in parallel planes, which is true for most OLEDs. The emitting organic layer is considered to be non-absorbing as absorption can suppress spontaneous emission from radiating dipoles [22]. As absorption of emissive layers (at emissive wavelengths) is considerably small it can be neglected without affecting accuracy [15].

Multiple emitting layers (interfaces) with independent anisotropy, independent emission locations, independent emission spectrum and independent distribution in emissive layer(s) can be simulated, this being very suitable for white (multi-color) devices. In many models [18, 23] only transmission to the exit medium (usually air) and total relative emission (Purcell factor) are presented, while in our model absorption of each individual layer can also be extracted. Due to the use of ray tracing in combination with TMM, multiple thick layers with thin-film stacks and various micro textures can be included in the simulations.

Another important advantage of our model is the possibility of simulating with restricted geometry in lateral dimensions. An entire device with independently limited emission and limited texture area can be simulated. This is very useful especially in research, where smaller samples are usually produced with limited emission area and limited texture area, see Figure 5 where only small pixel area is active and emits light while the texture is produced only above this pixel area. This can have immense effect on final results, thus limited area simulations are very beneficial for modeling realistic devices.

3 Experimental validation of the combined model

In this contribution, we present an experimental validation of the combined model on red bottom emitting p-i-n OLEDs (produced at TU Dresden) with flat and sine textured substrate / air interface. OLED structure with layer thicknesses is presented in Figure 1, while final device with visible laser structured sine texture can be seen in Figure 2. Sine textures were produced using laser structuring of the glass substrate – see Figure 5. Final textures are simple 1D sine textures with constant period P = 175 µm and three different heights h (2.5 µm, 6.5 µm and 15 µm). OLED production details can be found in [16, 24].

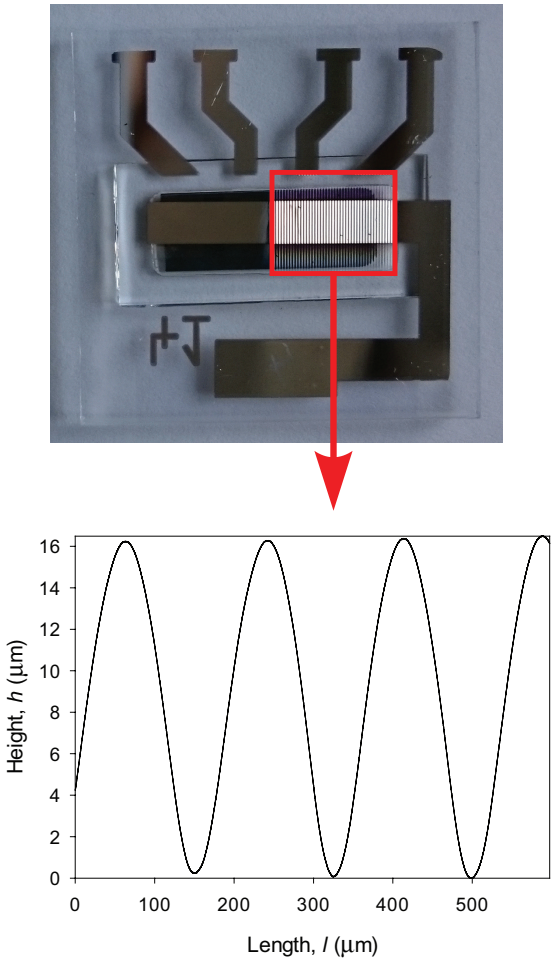

Figure 5: A produced bottom-emitting red OLED (four dots as indicated by the contacts) with sine textures on glass / air interface. Red rectangle indicates limited textured area of approx. 7x9 mm^2. Additionally, profilometer measurements of the sine textures for selected example is also shown.

Emitter material properties (γ= 0.92, $\eta_{rad,e}$ = 0.87, anisotropy a = 0.256, s_{el} – emission spectrum, emission positon) are taken from a previously published data [15] or gained from internal sources and were experimentally confirmed. The emission position was set at a single position in the emission layer with p = 1, the emission is still considered to be in emission layer, but infinitively close to the HBL (see Figure 1). Optical properties, in particular layer thicknesses and material refractive indices were supplied by TU Dresden and are within the anticipated error range.

Here we present comparison between simulations and experimental results for the total radiant intensity, *EQE* and AID which are important performance parameters of OLEDs. Comparison between simulations and experiment for total radiant intensity for flat and textured (sine textures with P = 175 µm and h = 15 µm) devices can be seen in Figure 6. Good matching between simulations and experiment can be observed, especially for the flat device. Some deviations are due to limited texture size in the experimental device (see Figure 5), as in simulations we simulated textured area as infinitive (this is justified for actual lightning applications since the emission and texture area are both large enough, more than 10x10 cm^2).

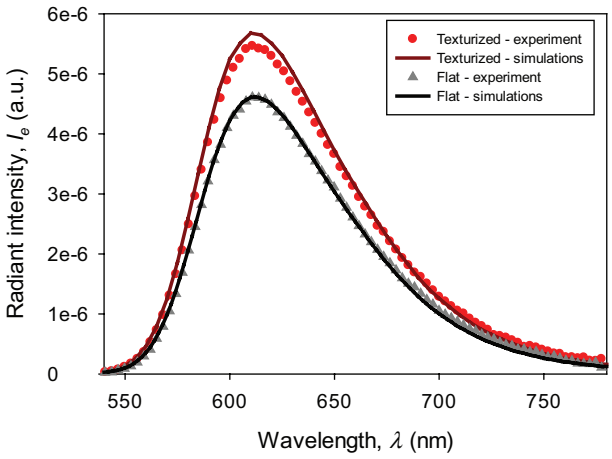

Figure 6: Comparison of total radiant intensity of a flat device and textured (sine textures with P = 175 µm and h = 15 µm) device for measurements and simulations.

We also compare measured and simulated *EQE*. The *EQE* was gained from AID measurements assuming rotation symmetry as:

$$EQE\left(I_c\right)=\frac{2\pi e}{I_c hc}\iint_{\vartheta\lambda}\lambda I_e\left(\vartheta,\lambda\right)\sin\vartheta d\vartheta d\lambda \qquad (14)$$

Where I_e is radiand intensity, I_c is applied current, e is elementary charge, c is the speed of light in vacuum, h is Planck constant and ϑ is a polar angle.

The *EQE* was calculated and simulated for a flat and a texturized OLED. The *EQE* of a flat OLED was taken as a reference and the gain (G) when using textures was defined as:

$$G=\frac{EQE_{\text{texturized}}-EQE_{\text{flat}}}{EQE_{\text{flat}}}*100\% \qquad (15)$$

We present here simulation and experimental results for 3 texturized OLED devices, with different sine aspect ratios (AR = h/P) of the textures. The results are presented in Table 1. Good matching was found again, minor deviations are due to limited texture size in experimental device (see Figure 5).

Table 1: Gain (*G*) comparison between experimental and simulation results for different *AR* of the sine textures.

Aspect ratio – *AR* (*h* (µm) / *P* (µm))	*G* (%) - experiment	*G* (%) - simulations
0 (0 / -)	0	**0**
0.0143 (2.5 / 175)	7.0	**9.0**
0.0371 (6.5 / 175)	11.2	**12.5**
0.0857 (15 / 175)	19.7	**20.6**

Another important parameter in OLEDs is the AID. We compare the simulated AID for flat and textured devices. Results for OLED with flat and texturized device (sine textures P = 175 µm, h = 15 µm) can be seen in Figure 7. Here we present an AID at emission peak wavelength of 610 nm. Comparing normalized simulated and experimental AID data from 0° to 60 °, deviations up to 2 % and up to 3 % can be found at individual angles for the flat and the textured device, respectively. While for angles over 60 ° where limited texture size (as light travelling under high angles in substrate does not fall on the textured surface entirely) starts to influence the measurement results, thus the difference rises up to 7 % and 15 % for flat and textured device, respectively. Only small deviations between simulation and experimental AID is identified and very good matching for flat and textured device can be observed.

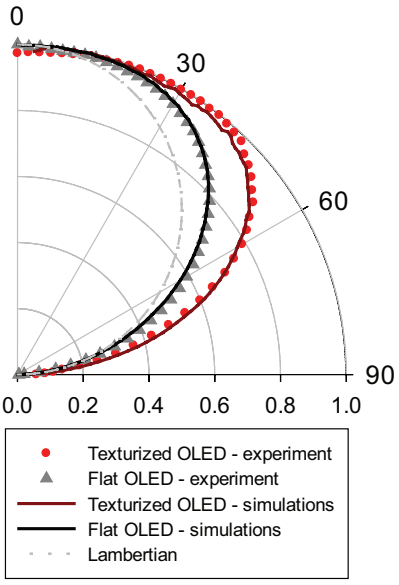

Figure 7: Angular intensity distribution (AID) comparison for flat and device with textured interface (sine textures on interface substrate/air with P = 175 µm and h = 15 µm) vs. simulation results for corresponding structures. Additionally, ideal Lambertian distribution is added.

4 Conclusions

A new combined optical model, based on TMM and ray-tracing approaches has been developed. Detailed modification of TMM to incorporate internal dipole sources was presented. TMM model with internal sources was combined with ray tracing simulator CROWM, to incorporate simulations of thick texturized layers. Dipoles as emission sources in OLEDs were applied to TMM formulations. OLEDs optical performance parameters - outcoupling efficiency and Purcell factor were gained using developed optical model and used in further calculations where good matching with experimental results was obtained. Additionally, simulated angular intensity distribution showed excellent matching with experimental results. The mismatch for angles up to 60° was under 3 %, for both flat and textured devices. In the final part, validation of the developed model was presented by comparison of simulated results with experimental ones. Good matching was obtained for red bottom-emitting p-i-n OLED devices on glass with flat and micro-textured front surface. Developed optical model accurately predicts optical behavior of flat and textured OLEDs and is appropriate for further simulations of advanced OLED devices. OLEDs with 1D front surface sine textures (textures were made by simple laser structuring of glass) outperform the flat counterpart in all performance parameters.

5 Acknowledgment

The authors acknowledge the financial support from the Slovenian Research Agency (P2-0197). M. Kovačič personally acknowledges the Slovenian Research Agency for providing PhD funding.

6 References

1. Y.-L. Chang and Z.-H. Lu, "White Organic Light-Emitting Diodes for Solid-State Lighting," *J. Disp. Technol.*, vol. 9, no. 6, pp. 459–468, Jun. 2013.
2. "NEC Lighting announces OLED Device with 156 Lm/W efficiency." [Online]. Available: http://www.osadirect.com/news/article/918/nec-lighting-announces-oled-device-with-156-lmw-efficiency/. [Accessed: 06-Mar-2015].
3. "Konica Minolta break their own record with world's most efficient OLED panel (139 lm/W)." [Online]. Available: http://www.oled-info.com/konica-minolta-break-their-own-record-worlds-most-efficient-oled-panel-139-lmw. [Accessed: 06-Mar-2015].

4. S. Reineke, M. Thomschke, B. Luessem, and K. Leo, "White organic light-emitting diodes: Status and perspective," *Rev. Mod. Phys.*, vol. 85, no. 3, pp. 1245–1293, Jul. 2013.
5. M. Jošt and M. Topič, "Efficiency limits in photovoltaics: Case of single junction solar cells," *Facta Univ. - Ser. Electron. Energ.*, vol. 27, no. 4, pp. 631–638, 2014.
6. R. Kimovec and M. Topič, "COMPARISON OF MEASURED PERFORMANCE AND THEORETICAL LIMITS OF GAAS LASER POWER CONVERTERS UNDER MONOCHROMATIC LIGHT," *Facta Univ. Ser. Electron. Energ.*, vol. 30, no. 1, pp. 93–106, Aug. 2016.
7. S. r. Forrest, D. d. c. Bradley, and M. e. Thompson, "Measuring the Efficiency of Organic Light-Emitting Devices," *Adv. Mater.*, vol. 15, no. 13, pp. 1043–1048, Jul. 2003.
8. J. Krc, B. Lipovsek, and M. Topic, "Design for high out-coupling efficiency of white OLED using CROWM - a combined geometric/wave optics model," in *Renewable Energy and the Environment (2013), paper JM3A.16*, 2013, p. JM3A.16.
9. L. Xiao, S.-J. Su, Y. Agata, H. Lan, and J. Kido, "Nearly 100% Internal Quantum Efficiency in an Organic Blue-Light Electrophosphorescent Device Using a Weak Electron Transporting Material with a Wide Energy Gap," *Adv. Mater.*, vol. 21, no. 12, pp. 1271–1274, Mar. 2009.
10. F. B. Dias *et al.*, "Triplet Harvesting with 100% Efficiency by Way of Thermally Activated Delayed Fluorescence in Charge Transfer OLED Emitters," *Adv. Mater.*, vol. 25, no. 27, pp. 3707–3714, Jul. 2013.
11. Q. Zhang *et al.*, "Nearly 100% Internal Quantum Efficiency in Undoped Electroluminescent Devices Employing Pure Organic Emitters," *Adv. Mater.*, vol. 27, no. 12, pp. 2096–2100, Mar. 2015.
12. K. Saxena, V. K. Jain, and D. S. Mehta, "A review on the light extraction techniques in organic electroluminescent devices," *Opt. Mater.*, vol. 32, no. 1, pp. 221–233, Nov. 2009.
13. W. Brütting, J. Frischeisen, T. D. Schmidt, B. J. Scholz, and C. Mayr, "Device efficiency of organic light-emitting diodes: Progress by improved light outcoupling," *Phys. Status Solidi A*, vol. 210, no. 1, pp. 44–65, Jan. 2013.
14. M. C. Gather and S. Reineke, "Recent advances in light outcoupling from white organic light-emitting diodes," *J. Photonics Energy*, vol. 5, p. 57607, May 2015.
15. M. Furno, R. Meerheim, S. Hofmann, B. Luessem, and K. Leo, "Efficiency and rate of spontaneous emission in organic electroluminescent devices," *Phys. Rev. B*, vol. 85, no. 11, p. 115205, Mar. 2012.
16. R. Meerheim, M. Furno, S. Hofmann, B. Luessem, and K. Leo, "Quantification of energy loss mechanisms in organic light-emitting diodes," *Appl. Phys. Lett.*, vol. 97, no. 25, p. 253305, Dec. 2010.
17. B. Lipovšek, J. Krč, and M. Topič, "Optical model for thin-film photovoltaic devices with large surface textures at the front side," *Inf. Midem*, vol. 41, no. 4, pp. 264–271, 2011.
18. K. A. Neyts, "Simulation of light emission from thin-film microcavities," *J. Opt. Soc. Am. -Opt. Image Sci. Vis.*, vol. 15, no. 4, pp. 962–971, Apr. 1998.
19. J. S. Orfanidis, *Electromagnetic Waves and Antennas*. Rutgers University, 2010.
20. A. Buckley, Ed., *Organic Light-Emitting Diodes*, 1 edition. Woodhead Publishing, 2013.
21. A. Čampa, *Modelling and optimization of advanced optical concepts in thin-film solar cells* Ljubljana: Založba FE in FRI, 2010.
22. M. S. Tomaš and Z. Lenac, "Decay of excited molecules in absorbing planar cavities," *Phys. Rev. A*, vol. 56, no. 5, pp. 4197–4206, Nov. 1997.
23. H. Benisty, R. Stanley, and M. Mayer, "Method of source terms for dipole emission modification in modes of arbitrary planar structures," *J. Opt. Soc. Am. -Opt. Image Sci. Vis.*, vol. 15, no. 5, pp. 1192–1201, May 1998.
24. M. Kovačič *et al.*, "Modelling of light outcoupling in OLEDs with sine textures," in *Conference proceedings 2016, 52nd International Conference on Microelectronics, Devices and Materials and the Workshop on Biosensors and Microfluidics*, Ankaran, Slovenia, 2016, vol. 2016, pp. 153–157.

Arrived: 20. 12. 2016
Accepted: 04. 01. 2017